reactions

MDPI

Article

Synthesis of Iodinated Cobalt Bis(dicarbollide) Conjugates with Acridine and Their Biological Studies

Nadezhda V. Dudarova [1], Egor V. Sidorskii [1], Anna I. Kasatova [2], Timofey A. Bykov [2], Yana V. Razdrogova [3], Dmitry S. Petrunya [3,4], Anastasia A. Antonets [5], Alexey A. Nazarov [5], Vsevolod A. Skribitsky [6], Anton A. Kasianov [6], Yulia A. Finogenova [6], Vladimir I. Lozinsky [1], Sergey Yu. Taskaev [2,7], Alexey A. Lipengolts [6], Sergey A. Anufriev [1], Anna A. Druzina [1,*], Igor B. Sivaev [1] and Vladimir I. Bregadze [1]

1 A.N. Nesmeyanov Institute of Organoelement Compounds, Russian Academy of Sciences, 28 Vavilov Str., 119334 Moscow, Russia
2 Budker Institute of Nuclear Physics, Siberian Branch, Russian Academy of Sciences, 11 Lavrentiev Prospect, 630090 Novosibirsk, Russia
3 P.N. Lebedev Physical Institute of the Russian Academy of Sciences, 53 Leninskiy Prospect, 119333 Moscow, Russia
4 National Research Centre "Kurchatov Institute", 1 Akademika Kurchatova pl., 123182 Moscow, Russia
5 Department of Chemistry, M.V. Lomonosov Moscow State University, 1/3 Leninskie Gory, 119991 Moscow, Russia
6 N.N. Blokhin National Medical Research Center of Oncology, 24 Kashirskoe Shosse, 115522 Moscow, Russia; b-f.finogenova@yandex.ru (Y.A.F.)
7 Novosibirsk State University, 2 Pirogov Str., 630090 Novosibirsk, Russia
* Correspondence: ilinova_anna@mail.ru; Tel.: +7-926-4045566

Abstract

Novel iodinated cobalt bis(dicarbollide) conjugates with acridine were synthesized by the direct iodination of cobalt bis(dicarbollide) conjugates with acridine using crystalline iodine. The cytotoxicity of the new compounds against various human cell lines was evaluated. One of these compounds was found to be non-toxic to all cell types and was combined with polyvinylpyrrolidone to form a non-covalent complex in order to increase its water solubility. The BNCT experiment showed that pre-incubation with the new boron-containing complex followed by neutron irradiation reduces the survival of T98G glioblastoma cells to 25% and B16 melanoma cells to 17%. The biodistribution of the boron-containing compound **5-PVP** was investigated in a B16F10 melanoma murine model. Maximum uptake in tumor and healthy tissues was observed 15 min after a single intravenous administration, and at 30 min post-injection the tumor/muscle ratio reached 5.4. This study lays the groundwork for further research on the development of methods for synthesizing acridine-based BNCT agents.

Keywords: iodinated cobalt bis(dicarbollide); acridine; polyhedral boron hydrides; poly(vinylpyrrolidone); in vivo study; boron neutron capture therapy

Check for updates

Academic Editor: Roberto Parise-Filho

Received: 29 August 2026
Revised: 24 October 2026
Accepted: 7 November 2026
Published: 16 November 2026

Copyright: © 2026 by the authors. Licensee MDPI, Basel, Switzerland. This article is an open access article distributed under the terms and conditions of the Creative Commons Attribution (CC BY) license.

1. Introduction

Cancer is a widespread disease that requires scientists to develop new, effective treatment methods [1–4]. Therefore, the development of drugs that can be used for cancer treatment is becoming increasingly important. One effective cancer treatment method is boron neutron capture therapy, the high potential of which has been demonstrated in both preclinical and clinical trials [5–11]. After administration of the drug, selective accumulation of non- radioactive ^{10}B boron atoms occurs in cancer cells, and subsequent thermal neutron irradiation induces the nuclear reaction $^{10}B + {}^{1}_{0}n \rightarrow [^{11}B]^* \rightarrow \alpha + {}^{7}Li + 2.31$ MeV, which produces an excited $[^{11}B]^*$ nucleus, which then decays into high linear energy transfer

(LET) particles, ^{4}He (α particles) and ^{7}Li [12–14]. The energy released by this reaction leads to the destruction of cancer cells [15,16]. However, the development of this method is hampered by the lack of effective drugs that can selectively penetrate and accumulate within cancer cells. This challenges scientists to develop boron-containing drugs with a number of specific characteristics.

The realization of a therapeutic effect in boron neutron capture therapy (BNCT) is contingent upon several critical prerequisites for potential pharmaceutical agents. These include the capacity for transmembrane penetration, selective targeting, and accumulation within neoplastic cells, and attainment of the requisite therapeutic boron concentration, conventionally defined as ≥20 μg ^{10}B/g of tumor [17–22]. Furthermore, it has been established that the radiobiological efficacy of the ^{10}B(n,α)^{7}Li capture reaction is substantially enhanced when the event occurs within the cell nucleus, as opposed to the cytoplasm or plasma membrane [23]. This intracellular localization is of particular significance, since nuclear confinement of BNCT drugs leads to more pronounced cellular destruction upon neutron irradiation than would be achieved with an equivalent boron load distributed homogeneously throughout the cell. Accordingly, targeted nuclear accumulation may allow the administered boron dose to be lowered, thereby reducing systemic toxicity [24]. These considerations have stimulated growing research interest in boron-functionalized DNA intercalators, including derivatives of phenanthridinium [25,26], naphthalimide [27–32], and related structural scaffolds [33].

An analysis of the literature revealed that acridine-based DNA intercalators are of great interest for medical applications [34,35]. Acridines and their derivatives are known to have a planar structure consisting of three conjugated six-membered rings. These structural features of acridine determine its intercalating properties and ability to bind to DNA and RNA molecules. The acridine moiety inserts between adjacent base pairs, altering the double helix structure. These structural distortions manifest as partial unwinding of the double helix and an increase in the vertical separation between neighboring base pairs at the intercalation site.

Consequently, acridine derivatives functionalized with polyhedral boron hydrides have attracted considerable interest as prospective BNCT agents. The synthetic chemistry of boron-containing acridines has been explored in several reported studies, wherein the boron moiety is typically represented by an *ortho*- or *para*-carborane framework [36–38]. More recently, a series of acridine conjugates bearing *ortho*- and *meta*-carborane clusters has been synthesized and evaluated with respect to their DNA-binding affinity and cytotoxic profiles [37,39,40]. In a complementary development, a conjugate of cobalt bis(dicarbollide) with acridine has been prepared; this compound exhibits low toxicity and holds promise as a candidate for BNCT applications [41]. Among the diverse family of polyhedral boron hydrides, the cobalt bis(dicarbollide) anion, [3,3′-Co(1,2-$C_2B_9H_{11}$)$_2$]$^-$ [40–46], has emerged as a particularly attractive boron delivery vehicle for BNCT, owing to its remarkable chemical robustness and favorable toxicological profile [47–50]. Notably, this metallacarborane possesses an amphiphilic character [51], which facilitates its passive permeation across lipid bilayer membranes and subsequent intracellular accumulation [20,52–55].

Furthermore, it is known that the introduction of halogens into the cobalt bis(dicarbollide) molecule improves cell penetration and helps achieve the required pharmacokinetic parameters [56,57]. In particular, the introduction of an iodine atom hinders ligand rotation through the formation of intramolecular C-H···I hydrogen bonds between the C-H groups of one dicarbollide ligand and the halogen substituent on the other [58,59]. Moreover, the presence of iodine facilitates transbilayer diffusion while concurrently reducing the propensity for nonspecific interactions with cellular components [52,55–58,60] and opens the way to radioiodine labeling for the determination of biodistribution in vivo [61,62]. The present

study was undertaken with the aim of synthesizing iodine-containing derivatives of cobalt bis(dicarbollide) with acridine. To achieve this goal, we used the iodination of previously obtained click-reaction conjugates of cobalt bis(dicarbollide) with acridine containing a triazole ring in the spacer.

2. Materials and Methods

2.1. Instruments, General Information and Synthetic Procedures

Conjugates **1–4** were prepared according to the literature procedures [63]. Iodine, CH_3OH, acetonitrile, CH_2Cl_2, $Na_2S_2O_3 \times 5H_2O$, and Na_2SO_4 were purchased from commercial vendors (Carl Roth GmbH, Karlsruhe, Germany; Abcr GmbH, Karlsruhe, Germany; Komponent-Reactiv, Moscow, Russia) and used without further purification. The reaction progress was monitored by thin-layer chromatography (Merck F254 silica gel on aluminum plates) and visualized using 0.5% $PdCl_2$ in 1% HCl in aq. MeOH (1:10). Macherey-Nagel Silica 60 (0.063–0.200 mm) column was used for column chromatography. The NMR spectra at 400.0 MHz (^{1}H), 128.3 MHz (^{11}B) and 100.6 MHz (^{13}C) were recorded on a Varian Inova 400 instrument equipped with a Qone QOT 400 X/HF-05 probe. The residual signal of the NMR solvent relative to TMS was taken as the internal reference for ^{1}H and ^{13}C{^{1}H} NMR spectra. ^{11}B and ^{11}B{^{1}H} NMR spectra were referenced against $BF_3 \times Et_2O$. The ^{11}B{^{1}H} spectra were used to determine the chemical shifts and signal intensities of the B-H and B-I groups; ^{11}B spectra were used to determine B-H coupling constants. Infrared spectra were recorded on an FSM2201 instrument (OKB SPECTRUM, Saint Petersburg, Russia). High-resolution mass spectra (HRMS) were measured on a micrOTOF II (Bruker Daltonics, Bremen, Germany) instrument using electrospray ionization (ESI). The measurements were performed in negative ion mode (interface capillary voltage 3000 V), with a mass range from m/z 50 to m/z 3000; external or internal calibration was carried out with ESI Tuning Mix (Agilent). Syringe injection was used for solutions in acetonitrile (flow rate 3 μL/min). Nitrogen was used as the drying gas; the interface temperature was set at 180 °C. Elemental analyses were performed at the Laboratory of Microanalysis of the A.N. Nesmeyanov Institute of Organoelement Compounds.

General Method for the Synthesis of Iodinated Cobalt Bis(dicarbollide) Conjugates with Acridine (5–8). Crystalline iodine (3 equiv.) was added to CH_3OH and stirred for three hours until complete dissolution. Then, the solution was added to the conjugate of cobalt bis(dicarbollide) with acridine **1–4**, and the mixture was refluxed for three hours. The reaction mixture was cooled, and the solvent was evaporated. The residue was extracted with ethyl acetate, and the extract was washed with an aqueous solution of $Na_2S_2O_3 \times 5H_2O$ (2 × 50 mL) and H_2O (2 × 50 mL). The organic layer was dried over anhydrous Na_2SO_4. The inorganic precipitate was filtered off, and the solvent was evaporated.

Synthesis of [p-{8-NHCH$_2$CH$_2$-N$_3$CHC-CH$_2$O(CH$_2$CH$_2$O)$_2$-8′-I-3,3′-Co(1,2-C$_2$B$_9$H$_{10}$)(1′,2′-C$_2$B$_9$H$_{10}$)}-(C$_6$H$_4$)$_2$[b,e]pyridinate]Cs (**5**). Obtained from 120 mg (0.14 mmol) of compound **1**, 100 mg (0.42 mmol) of crystalline I_2, and 70 mL of CH_3OH. The yield of product **5** was 100 mg (88%), an orange solid. NMR ^{1}H (400 MHz, acetone-d_6) δ, ppm: 8.54 (d, 2H, J = 9.0 Hz, CH_{Ar}), 8.03 (t, 2H, J = 7.8 Hz, CH_{Ar}), 7.96 (s, 1H, CHCN$_3$), 7.92 (d, 2H, J = 8.7 Hz, CH_{Ar}), 7.64 (t, 2H, J = 8.0 Hz, CH_{Ar}), 5.10 (t, 2H, J = 5.1 Hz, CH_2N), 4.91 (t, 2H, J = 5.2 Hz, CH_2N), 4.51 (s, 2H, OCH_2CCHN$_3$), 4.41 (br.s, 2H, CH_{Carb}), 4.13 (br.s, 2H, CH_{Carb}), 3.55 (m, 4H, 2 × CH_2O), 3.46 (m, 4H, 2 × CH_2O). ^{11}B NMR (128 MHz, acetone-d_6) δ, ppm: 21.5 (s, 1B, B-O), −0.4 (d, 2B, J = 119 Hz, B-H), −5.9 (m, 9B, J = 119 Hz, B-H + B-I), −17.9 (d, 2B, J = 162 Hz, B-H), −19.9 (d, 2B, J = 151 Hz, B-H), −23.1 (d, 1B, J = 142 Hz, B-H), −27.0 (d, 1B, J = 142 Hz, B-H). ^{13}C{^{1}H} NMR (101 MHz, acetone-d_6) δ, ppm: 159.7 (C_{Ar}), 146.0 (C_{Ar}), 140.6 (CCHN$_3$), 136.6 (CH$_{Ar}$), 126.1 (CH$_{Ar}$), 125.3 (CH$_{Ar,}$), 125.1 (CCHN$_3$), 119.8 (CH$_{Ar}$), 113.8 (C_{Ar}), 72.7 (OCH$_2$), 71.1 (OCH$_2$), 70.4 (OCH$_2$), 69.1

(OCH_2), 64.9 (OCH_2CCHN_3), 57.3 (CH_{Carb}), 55.4 (CH_{Carb}), 50.1 (CH_2N), 49.9 (CH_2N). IR (film, cm^{-1}): 2566 (υ_{B-H}), 1582 (υ_{triaz}). Found: C 36.71, H 5.23, B 22.82, N 8.39; calcd: C 36.52, H 5.19, B 22.76, N 8.19. HRMS (ESI) of $C_{26}H_{44}B_{18}CoIN_5O_3$, *m*/*z*: calcd for $[M + H]^+$ 855.3625, found: 855.3624.

Synthesis of [p-{8-NHCH$_2$CH$_2$-N$_3$CHC-CH$_2$CH$_2$O(CH$_2$CH$_2$O)$_2$-8′-I-3,3′-Co(1,2-C$_2$B$_9$H$_{10}$)(1′,2′-C$_2$B$_9$H$_{10}$)}-(C$_6$H$_4$)$_2$[b,e]pyridinate]Cs (**6**). Obtained from 230 mg (0.26 mmol) of compound **2**, 200 mg (0.78 mmol) of crystalline I_2, and 90 mL of CH_3OH. The yield of product **6** was 220 mg (84%), an orange solid. NMR ^1H (400 MHz, acetone-d_6) δ, ppm: 8.54 (d, 2H, *J* = 8.8 Hz, CH_{Ar}), 8.05 (t, 2H, *J* = 7.8 Hz, CH_{Ar}), 7.95 (d, 2H, *J* = 8.0 Hz, CH_{Ar}), 7.87 (s, 1H, $CHCN_3$), 7.65 (m, 2H, *J* = 7.8 Hz, CH_{Ar}), 5.07 (t, 2H, *J* = 5.3 Hz, CH_2N), 4.89 (t, 2H, *J* = 5.1 Hz, CH_2N), 4.45 (br.s, 2H, CH_{Carb}), 4.16 (br.s, 2H, CH_{Carb}), 3.59 (t, 2H, *J* = 6.3 Hz, $OCH_2CH_2CCHN_3$), 3.50 (m, 6H, 3 × OCH_2), 3.44 (m, 2H, OCH_2), 2.84 (t, 2H, *J* = 6.5 Hz, CH_2CCHN_3). ^{11}B NMR (128 MHz, acetone-d_6) δ, ppm: 21.5 (s, 1B, B-O), −0.7 (d, 2B, *J* = 125 Hz, B-H), −5.8 (m, 9B, B-H + B-I), −17.9 (d, 2B, *J* = 148 Hz, B-H), −20.0 (d, 2B, *J* = 167 Hz, B-H), −23.1 (d, 1B, *J* = 147 Hz, B-H), −27.3 (d, 1B, *J* = 176 Hz, B-H). $^{13}C\{^1H\}$ NMR (101 MHz, acetone-d_6) δ, ppm: 159.5 (C_{Ar}), 147.4 (C_{Ar}), 142.0 ($CCHN_3$), 136.6 (CH_{Ar}), 126.1 (CH_{Ar}), 125.3 (CH_{Ar}), 124.2 ($CCHN_3$), 119.7 (CH_{Ar}), 113.7 (C_{Ar}), 72.6 (OCH_2), 71.0 (OCH_2), 70.7 (OCH_2), 70.4 ($OCH_2CH_2CCHN_3$), 69.2 (OCH_2), 57.3 (CH_{Carb}), 55.4 (CH_{Carb}), 50.1 (CH_2N), 49.6 (CH_2N), 27.1 (CH_2CCHN_3). IR (film, cm^{-1}): 2564 (υ_{B-H}), 1583 (υ_{triaz}). Found: C 32.74, H 4.79, B 19.64, N 7.12; calcd: C 32.36, H 4.63, B 19.42, N 6.99. HRMS (ESI) of $C_{27}H_{46}IB_{18}CoN_5O_3$, *m*/*z*: calcd for $[M + H]^+$ 869.3782, found: 869.3781.

Synthesis of [p-{8-NHCH$_2$CH$_2$-N$_3$CHC-CH$_2$O(CH$_2$)5O-8′-I-3,3′-Co(1,2-C$_2$B$_9$H$_{10}$)(1′,2′-C$_2$B$_9$H$_{10}$)}-(C$_6$H$_4$)$_2$[b,e]pyridinate]Cs (**7**). Obtained from 270 mg (0.31 mmol) of compound **3**, 240 mg (0.93 mmol) of crystalline I_2, and 90 mL of CH_3OH. The yield of product **7** was 270 mg (85%), an orange solid. NMR ^1H (400 MHz, acetone-d_6) δ, ppm: 8.56 (d, 2H, *J* = 9.1 Hz, CH_{Ar}), 8.02 (m, 3H, CH_{Ar} + $CHCN_3$), 7.94 (d, 2H, CH_{Ar}, *J* = 9.0 Hz), 7.63 (m, 2H, CH_{Ar}), 5.14 (m, 2H, CH_2N), 4.94 (m, 2H, CH_2N), 4.47 (s, 2H, OCH_2CCHN_3), 4.32 (br.s, 2H, CH_{Carb}), 4.18 (br.s, 2H, CH_{Carb}), 3.38 (t, 2H, *J* = 5.9 Hz, OCH_2), 3.33 (t, 2H, *J* = 5.0 Hz, OCH_2), 1.47 (m, 2H, CH_2), 1.40 (m, 2H, CH_2), 1.28 (m, 2H, CH_2). ^{11}B NMR (128 MHz, acetone-d_6) δ, ppm: 21.7 (s, 1B, B-O), −0.6 (d, 2B, *J* = 136 Hz, B-H), −6.5 (m, 9B, B-H + B-I), −18.0 (d, 2B, *J* = 157 Hz, B-H), −19.9 (d, 2B, *J* = 163 Hz, B-H), −23.4 (d, 1B, *J* = 159 Hz, B-H), −27.4 (d, 1B, *J* = 158 Hz, B-H). $^{13}C\{^1H\}$ NMR (101 MHz, acetone-d_6) δ, ppm: 159.5 (C_{Ar}), 146.4 (C_{Ar}), 140.7 ($CCHN_3$), 136.6 (CH_{Ar}), 126.2 (CH_{Ar}), 125.3 (CH_{Ar}), 124.9 ($CCHN_3$), 119.7 (CH_{Ar}), 113.7 (C_{Ar}), 70.9 (OCH_2), 69.4 (OCH_2), 64.7 (OCH_2CCHN_3), 57.3 (CH_{Carb}), 55.2 (CH_{Carb}), 50.0 (CH_2N), 49.7 (CH_2N), 32.3 (CH_2), 30.1 (CH_2), 23.5 (CH_2). IR (film, cm^{-1}): 2555 (υ_{B-H}), 1583 (υ_{triaz}). Found: C 33.13, H 4.91, B 19.85, N 7.27; calcd: C 32.89, H 4.70, B 19.73, N 7.10. HRMS (ESI) of $C_{27}H_{46}IB_{18}CoN_5O_2$, *m*/*z*: calcd for $[M + H]^+$ 853.3833, found: 853.3831.

Synthesis of [p-{8-NHCH$_2$CH$_2$-N$_3$CHC-CH$_2$CH$_2$O(CH$_2$)$_5$O-8′-I-3,3′-Co(1,2-C$_2$B$_9$H$_{10}$)(1′,2′-C$_2$B$_9$H$_{10}$)}-(C$_6$H$_4$)$_2$[b,e]pyridinate]Cs (**8**). Obtained from 100 mg (0.11 mmol) of compound **4**, 80 mg (0.33 mmol) of crystalline I_2, and 40 mL of CH_3OH. The yield of product **8** was 90 mg (81%), an orange solid. NMR ^1H (400 MHz, acetone-d_6) δ, ppm: 8.55 (d, 2H, *J* = 9.0 Hz, CH_{Ar}), 8.06 (t, 2H, *J* = 7.7 Hz, CH_{Ar}), 7.95 (d, 2H, *J* = 9.1 Hz, CH_{Ar}), 7.84 (s, 1H, $CHCN_3$), 7.66 (t, 2H, *J* = 7.7 Hz, CH_{Ar}), 5.09 (m, 2H, CH_2N), 4.90 (m, 2H, CH_2N), 4.33 (br.s, 2H, CH_{Carb}), 4.19 (br.s, 2H, CH_{Carb}), 3.51 (t, 2H, *J* = 6.2 Hz, $OCH_2CH_2CCHN_3$), 3.31 (t, 2H, *J* = 6.2 Hz, 2 × OCH_2), 2.83 (m, 2H, CH_2CCHN_3), 1.40 (m, 4H, 2 × CH_2), 1.28 (m, 4H, CH_2). ^{11}B NMR (128 MHz, acetone-d_6) δ, ppm: 21.8 (s, 1B, B-O), −0.6 (d, 2B, *J* = 141 Hz, B-H), −5.9 (m, 9B, B-H + B-I), −18.0 (d, 2B, *J* = 162 Hz, B-H), −19.9 (d, 2B, *J* = 146 Hz, B-H), −23.5 (d, 1B, *J* = 158 Hz, B-H), −27.5 (d, 1B, *J* = 154 Hz, B-H). $^{13}C\{^1H\}$ NMR (101 MHz, acetone-d_6) δ, ppm: 159.6 (C_{Ar}), 146.3 (C_{Ar}), 140.7 ($CCHN_3$), 136.7 (CH_{Ar}),

126.2 (CH_{Ar}), 125.3 (CH_{Ar}), 124.1 ($CCHN_3$), 119.7 (CH_{Ar}), 113.7 (C_{Ar}), 71.3 (OCH_2), 70.1 ($OCH_2CH_2CCHN_3$), 69.5 (OCH_2), 57.3 (CH_{Carb}), 55.2 (CH_{Carb}), 50.2 (CH_2N), 49.6 (CH_2N), 32.3 (CH_2), 30.2 (CH_2), 27.2 (CH_2CCHN_3), 23.6 (CH_2). IR (film, cm^{-1}): 2553 (υ_{B-H}), 1583 (υ_{triaz}). Found: C 33.63, H 4.84, B 19.46, N 7.00; calcd: C 33.89, H 5.02, B 19.89, N 7.19. HRMS (ESI) of $C_{27}H_{46}IB_{18}CoN_5O_2$, *m*/*z*: calcd for $[M + H]^+$ 867.3990, found: 867.3991.

Preparation of **5-*PVP*** *Non-Covalent Complex*

160 mg of compound **5** was suspended in 8 mL of EtOH and stirred for 4 h at 56 °C until complete dissolution. The resultant solution was further mixed with 70 mL of aqueous PLASDONE® K-17 (ISP Technologies Inc., Waterford, MI, USA) solution ([PVP] = 10 mg/mL), placed in a 100 mm Petri dish, frozen at −28 °C for 24 h, and then lyophilized using a FreeZone freeze-dryer (Labconco, Kansas City, MO, USA). The content of compound **5** in the sample was measured by spectrophotometry using a UV-Vis spectrophotometer (OKB SPECTRUM, Saint Petersburg, Russia) at a wavelength of 264 nm.

2.2. Cells and Mtt Assay

The human HCT116 colorectal carcinoma, MCF7 breast adenocarcinoma, A549 non-small cell lung carcinoma, and WI38 nonmalignant lung fibroblast cell lines were obtained from the European Collection of Authenticated Cell Cultures (ECACC; Salisbury, UK). All cells were grown in DMEM medium (Gibco™, Grand Island, NE, USA) supplemented with 10% fetal bovine serum (Gibco™, Sao Paolo, Brazil). The cells were cultured in an incubator at 37 °C in a humidified 5% CO_2 atmosphere and subcultured twice a week. The MTT (3-(4,5-dimethylthiazol-2-yl)-2,5-diphenyltetrazolium bromide) assay was performed as described earlier [64]. In brief, the cells were seeded in 96-well plates (TPP, Trasadingen, Switzerland) at a density of 1×10^4 cells/well in 100 µL. After a 24 h incubation at 37 °C, the cells were treated with the test compounds at concentrations ranging from 0 to 200 µM.

2.3. Boron Neutron Capture Therapy in Vitro

Three cell lines were used in the BNCT studies: B16 mouse skin melanoma, obtained at the Institute of Cytology and Genetics SB RAS (Novosibirsk), and two human cell lines T98G (glioblastoma) and DF1 (dermal fibroblasts), obtained from the Russian Collection of Vertebrate Cell Cultures at the Institute of Cytology RAS (St. Petersburg). The cells were cultured in DMEM/F12 medium (Biolot, Saint Petersburg, Russia) supplemented with 10% fetal bovine serum (DiaM, Moscow, Russia) and penicillin-streptomycin antibiotics (Biolot, Russia) at 37 °C in a humidified 5% CO_2 atmosphere. The cells were subcultured three times a week.

Since preliminary cytotoxicity experiments with the iodinated cobalt bis(dicarbollide) conjugates with acridine **5–8** against a number of cell lines revealed no antiproliferative activity (IC_{50}) against any of the cell lines studied (except for compound **5**), it was decided to investigate the effect of compound **5-PVP** on the viability of the B16 line over a wide range of boron-10 concentrations. The MTT test was performed as described previously [65,66].

To assess boron accumulation, B16 cells were seeded into culture flasks, with 3 replicates for each experimental point, and incubated for 24 h. The test boron-containing compound was added at a concentration of 40 µg/mL, and the cells were incubated with it for 24 h, after which the cells were counted and centrifuged. The cell pellets were digested with concentrated nitric acid at 90 °C for 2 h; the samples were then left for 24 h at room temperature. The analysis was performed by ICP-AES using an ICPE-9820 spectrometer (Shimadzu, Kyoto, Japan).

Before the BNCT experiment, B16, T98G, and DF1 cells were seeded into culture flasks; the boron delivery agent **5-PVP** with a boron-10 concentration of 40 µg/mL was added to the "BNCT" and "5-PVP" groups. The "control" and "irradiation" groups were incubated

without boron-containing compounds. Before irradiation, the cells were washed and placed in cryotubes (Biologix, Jinan, China). The cryotubes with cells from the "irradiation" and "BNCT" groups were placed in a phantom made of polymethyl methacrylate, designed for in vitro experiments. The phantom was positioned beneath a Poly-Biz moderator with a thickness of 72 mm. The irradiation was carried out for 30 min with a proton energy of 2.0 MeV and a current integral of 1 mA × h at the accelerator-based neutron source VITA at the Budker Institute of Nuclear Physics, Novosibirsk [67].

The irradiation parameters of the cell cultures were evaluated in the Geant4 software toolkit (version 11.2.1) using the QGSP_BIC_AllHP physics list and the developed model of the neutron-generating system of the VITA accelerator-based neutron source [68,69].

For the MTT assay, 5×10^3 cells per well were seeded into 96-well plates and incubated for 4 days. The test was performed according to the procedure described above.

To assess cell migration after irradiation, culture inserts were placed into a 24-well plate, and 5×10^3 cells in 100 µL of medium were seeded into each well of the insert. After 24 h, the inserts were removed, the wells were washed, and complete culture medium was added. Micrographs were taken 1 day and 3 days after BNCT (magnification ×100).

For the clonogenic assay, 200 cells per well were seeded into a 6-well plate. Colonies were stained using 6% glutaraldehyde (Neofroxx, Einhausen, Germany) and a 0.5% aqueous solution of crystal violet (DiaM, Moscow, Russia). Colony counting was performed using an inverted light microscope (Olympus, Hachioji-shi, Japan); a colony was defined as a clone containing more than 50 cells.

Data were statistically processed using STATISTICA 10.0 software. For the separate MTT cytotoxicity test of **5-PVP** comparisons among concentrations, one-way analysis of variance (ANOVA) followed by Dunnett's post-hoc test against the control group was performed. Comparisons among groups after BNCT were performed using one-way ANOVA followed by Tukey's post-hoc test for multiple comparisons. Results are presented as mean ± standard deviation (M ± SD) from three independent experiments; technical replicates were averaged within each independent experiment before analysis. Differences were considered statistically significant at $p < 0.05$.

2.4. Ex Vivo Biodistribution Study and Tumor Uptake

All procedures involving animals were performed in accordance with local ethical regulations and approved by the institutional ethical committee (protocol No. 2026-5.1, issued on 15.05.2026). Female C57Bl/6 mice weighing 20–22 g (obtained from the Animal Breeding Facility of the N.N. Blokhin National Medical Research Center of Oncology) were used in this study. Melanoma B16F10 cells (obtained from the cryobank of the N.N. Blokhin National Medical Research Center of Oncology) were transplanted subcutaneously into the right flank of the animals. Inoculation was performed using 0.2 mL of an *ex tempore* prepared 14% (*w*/*v*) tumor cell suspension in Hanks' solution.

At a tumor volume of 0.2–0.4 cm^3, the animals were randomly divided into 5 groups of 5 animals each. All mice received a single intravenous injection of 0.2 mL of the **5-PVP** compound at a concentration of 214 µg B/mL, which corresponded to ~2 mg B/kg bw. At 15, 30, 60, 90, and 120 min post-injection, the respective groups were euthanized by isoflurane overdose. Immediately after euthanasia, the following organs and tissues were collected: blood, tumor, muscle, skin, liver, kidneys, heart, lungs, spleen, and brain. All tissue samples except blood were rinsed in distilled water, dried, and weighed. After collection, the samples were stored at −20 °C until further analysis.

For elemental analysis, tissue samples (0.2–1.0 g) were mineralized by microwave-assisted digestion in an Ethos Easy system (MILESTONE, Sorisole, Italy) using 5 mL of concentrated HNO_3 and 1 mL of H_2O_2. The temperature was gradually raised to 190 °C

over 30 min and maintained at 190 °C for 10 min. After cooling to 50 °C, the digestate was transferred to 50 mL boron-free plastic Falcon tubes, supplemented with 50 µL of Triton X-100, and diluted.

Total boron concentrations were determined by inductively coupled plasma optical emission spectrometry (ICP-OES) using a PlasmaQuant 9100 Series spectrometer (Analytik Jena, Jena, Germany). Measurements were performed in triplicate at two emission wavelengths: 249.773 nm and 249.678 nm. Calibration was performed using a multi-element standard solution IV (Supelco). The calibration curve was linear in the range of 0.02–12 µg B/mL with $R^2 > 0.99$. Final concentrations were calculated taking into account the dilution to 10 mL with deionized water during sample preparation.

Data are presented as mean ± standard deviation (M ± SD). Boron concentrations were compared across five time points (15, 30, 60, 90 and 120 min) using one-way analysis of variance (ANOVA). Where significant effects were detected, post-hoc pairwise comparisons were performed using Tukey's honestly significant difference test to control the family-wise error rate. Statistical significance was set at $p < 0.05$. All analyses were conducted using JASP 0.97.1.

3. Results and Discussion

3.1. Chemistry

Modification of polyhedral boron hydrides with acridine allows for the production of derivatives that combine the unique properties of boron clusters with the exceptional characteristics of acridine. In this context, it is noteworthy that N^9-substituted acridine derivatives, by virtue of their unique chemical architecture, display a broad spectrum of biological activities [70]. In particular, 9-aminoacridines have been shown to accumulate selectively in cell nuclei and in other DNA- and RNA-containing subcellular compartments. Currently, the clinically approved antitumor agent amsacrine, an N^9-substituted acridine derivative, remains in active use for the treatment of various leukemias [71], and its structural analogues continue to be the subject of intensive investigation [72]. Structural studies of N^9-substituted acridines further indicate that the introduction of substituents at the 9-amino group attenuates the intrinsic toxicity of these compounds [72]. These observations provide a compelling rationale for the design of novel potential BNCT agents wherein a boron-rich fragment, containing up to 18 boron atoms per molecule, is attached to the acridine scaffold *via* the N^9 position of the aromatic system. This strategy has previously been exemplified by the synthesis of cobalt bis(dicarbollide)-acridine conjugates employing a copper(I)-catalyzed azide-alkyne cycloaddition ("click" reaction) between an azido derivative of acridine and terminal alkynes of cobalt bis(dicarbollide) [63]. In this article, we describe the modification of acridine with iodinated cobalt bis(dicarbollide) at the N^9 position of the aromatic system (Figure 1).

To obtain iodine-containing conjugates of cobalt bis(dicarbollide) with acridine, iodination of 1,2,3-triazoles **1–4** with an excess of crystalline I_2 was carried out in refluxing MeOH for three hours, leading to the formation of new derivatives **5–8** in 81–88% yields (Scheme 1), which can potentially be used as effective BNCT agents. The structures of conjugates **5–8** were confirmed by ^1H, $^{11}B\{^1H\}$, ^{11}B, and $^{13}C\{^1H\}$ NMR spectroscopy, IR spectroscopy, and high-resolution mass spectrometry (see Supplementary Materials, Figures S1–S31).

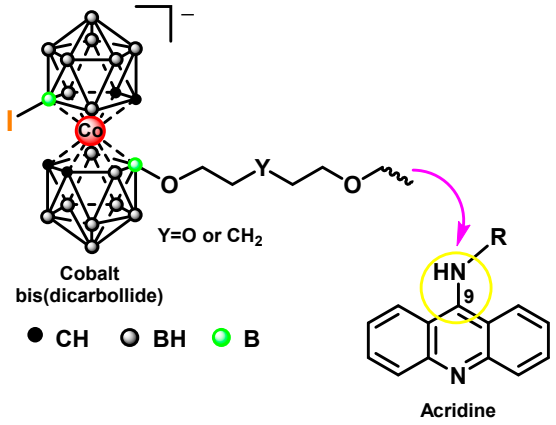
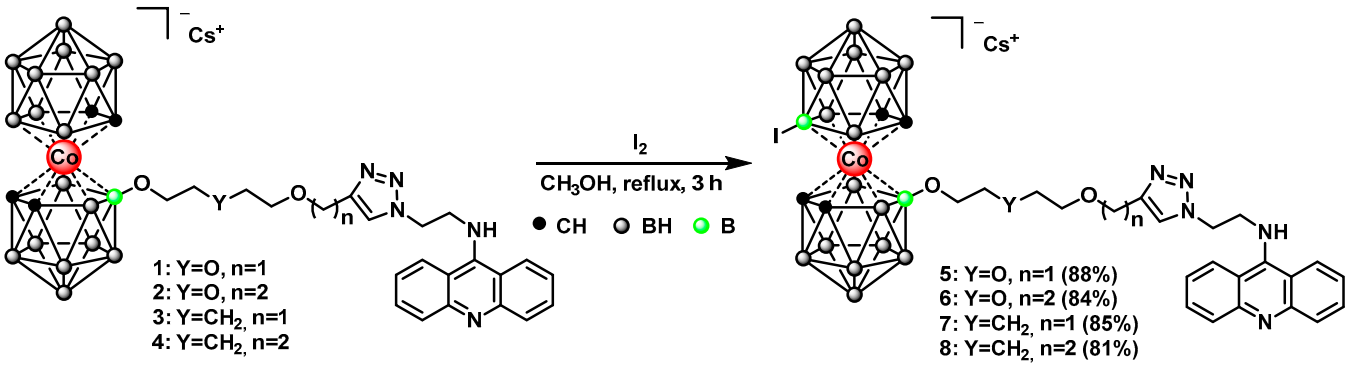


Figure 1. The structure of N^9-substituted acridine.



Scheme 1. The synthesis of iodinated cobalt bis(dicarbollide) conjugates with acridine **5–8**.

The ^{1}H NMR spectra of conjugates **5–8** contain the characteristic signals of the triazole CH group at 7.84–8.01 ppm, signals of acridine CH groups at 7.63–8.56 ppm, and signals of carborane CH groups at 4.13–4.45 ppm. In the ^{13}C{^{1}H} NMR spectra, characteristic signals of the triazole CH and C groups at 124.1–125.1 and 140.6–142.0 ppm, signals of the acridine CH, C, and C-N groups at 119.7–136.7, 146.0–159.7, and 113.7–113.8 ppm, and signals of the carborane CH groups at 55.2–57.3 ppm, respectively, are observed. In the NMR ^{11}B{^{1}H} spectra of compounds **5–8**, the B-O signals are present at approx. 21.6 ppm, and the B-I signals overlap with the group of BH signals in the region of −6.0 ppm, as expected for such cobalt bis(dicarbollide) derivatives.

The IR spectra of compounds **5–8** show a strong B-H stretching band at ~2565 cm^{-1}.

3.2. Biological Properties

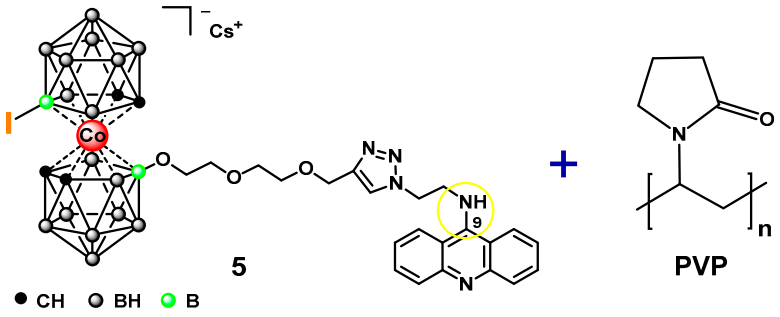
3.2.1. Cytotoxic Activity of Conjugates of Iodinated Cobalt Bis(dicarbollide) with Acridine **5–8**

The cytotoxic effects of compounds **5–8** against human cancer cell lines HCT116, MCF7, and A549, alongside nonmalignant WI38 lung fibroblasts, were assessed using a standard MTT colorimetric assay after a 72 h incubation period (Table 1). Compound **5** was non-toxic (IC_{50} > 100 μM) across all tested cell lines. All four compounds were found to be non-toxic toward the A549 lung cancer cell line and the WI38 normal fibroblast line. In contrast, compounds **6**, **7**, and **8** exhibited mid-micromolar cytotoxic activity against the HCT116 and MCF7 lines, which restricts their suitability as potential agents for BNCT.

Table 1. Cytotoxic activity of conjugates of cobalt bis(dicarbollide) with acridine **5–8** against A549, HCT116, MCF-7, and WI-38 cells after a 72-h exposure; cisplatin served as a reference compound. The results are the mean values ± SD of three independent experiments, each of which was done in triplicate.

Cell Line	Cytotoxicity IC_{50}, μM.				
	5	**6**	**7**	**8**	**Cisplatin [57]**
WI38	>100	>100	>100	>100	8 ± 3
A549	>100	>100	>100	>100	13 ± 3
HCT116	>100	21 ± 9	63 ± 6	53 ± 4	13 ± 4
MCF7	>100	44 ± 8	45 ± 4	22 ± 4	30 ± 9

Based on the data obtained, it was decided to select conjugate **5** for further biological studies. It has previously been shown that the water solubility of cobalt bis(dicarbollide) derivatives can be increased by using suitable biocompatible excipients, i.e., carriers of pharmaceutically active compounds, including poly(vinylpyrrolidone) (PVP) [73,74]. Specifically, to increase the water solubility of compound **5**, it was converted into a non-covalent complex with PVP (Scheme 2). This resulted in a water-soluble form, **5-PVP**, which was used to determine cytotoxicity and intracellular accumulation, and in the BNCT experiment in vitro.



Scheme 2. The non-covalent complex of poly(vinylpyrrolidone) with iodinated cobalt bis(dicarbollide) conjugate with acridine **5-PVP**.

The fabrication of **5-PVP** was performed in accordance with a patented procedure [75,76]. In the case of **5-PVP**, the procedure included dissolution of compound **5** in ethanol and of **PVP** (MW 10 kDa) in water, mixing of these solutions, freezing of the resulting liquid system, and its subsequent freeze-drying (see Section 2). The conjugate content of the **5-PVP** sample was 19.7 wt%, and its water solubility reached 250 mg/mL. The solid matter thus produced was shown to possess at least 100-fold higher solubility in aqueous media at physiological pH than compound **5** itself. Thus, we used a derivative based on cobalt bis(dicarbollide), in which the natural abundance of the boron-10 isotope is 20%.

3.2.2. Cytotoxicity, Intracellular Accumulation and Bnct Experiment in Vitro of **5-PVP**

The cytotoxicity of **5-PVP** toward the B16 cell line at various boron-10 concentrations is presented in Figure 2.

During the first 24 h of incubation of **5-PVP** with B16 cells, no decrease in viability was observed; a slight, statistically insignificant increase in viability during incubation with high concentrations may be associated with an interaction between PVP and MTT. Upon longer incubation, a significant decrease in viability occurred even at the lowest concentration used, which indicates that incubation with **5-PVP** is safe for no more than 24 h at boron-10 concentrations up to 125 μg/mL.

The boron content in the B16 cells was 0.98 ± 0.08 μg/10^6 cells. Taking into account the natural abundance of the boron-10 isotope (20%), the boron-10 content is 0.20 μg/10^6 cells.

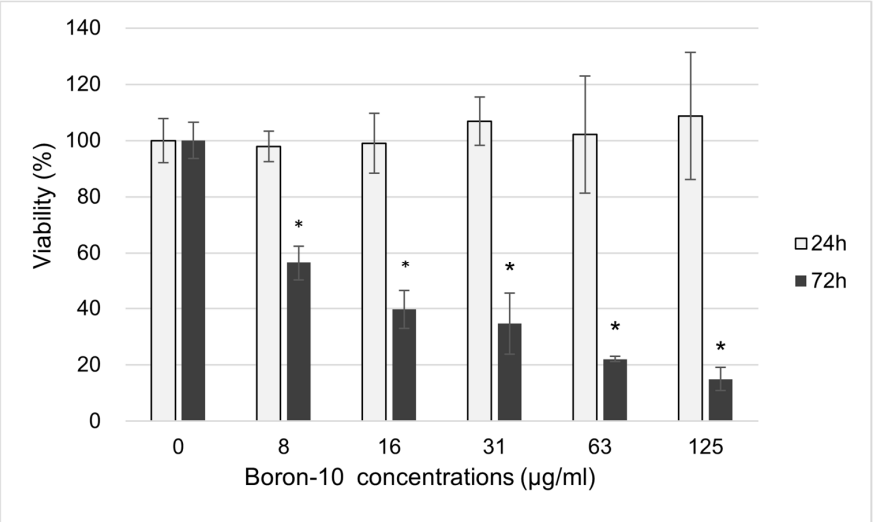


Figure 2. Cytotoxicity of **5-PVP** toward the B16 cell line. *—$p < 0.05$ versus the control group (one-way ANOVA followed by Dunnett's post-hoc test, $n = 3$ independent experiments).

Three different cell tests to detect the radiation-induced impairment were used: the migration test, the MTT test reflecting metabolic activity, and a clonogenic assay indicating colony-forming capacity.

The cell viability results are shown in Figure 3. No pronounced effect of irradiation in the presence of the new boron-containing compound **5-PVP** on the B16 and DF1 cell lines was observed compared to the other groups. A statistically significant reduction in the viability of T98G cells was observed, with a survival rate of 71%.

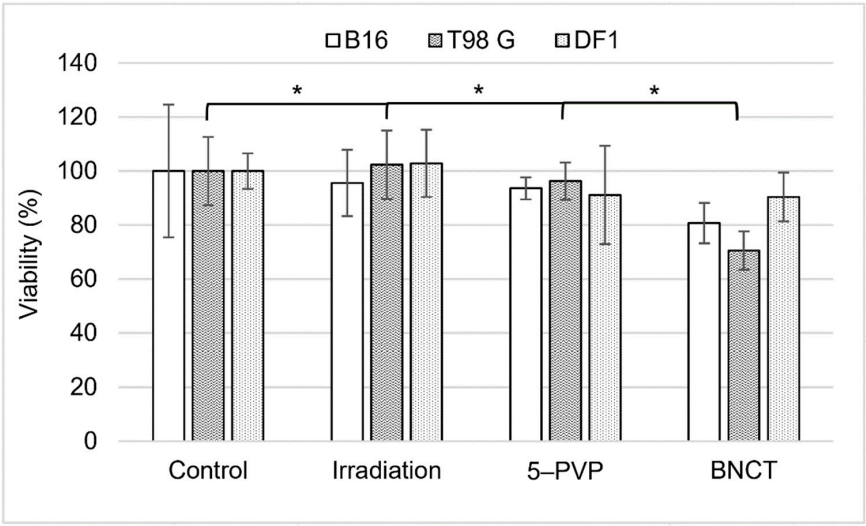


Figure 3. Cytotoxicity indicators for different types of exposure: neutron irradiation, the drug alone, and BNCT. MTT assay 96 h after BNCT with **5-PVP**. *—$p < 0.05$ versus the control group (one-way ANOVA followed by Tukey's post-hoc test, $n = 3$ independent experiments).

A 96-h time interval was selected for the MTT assay, since by this point the cells are considered to have already undergone several division attempts. When the assay is performed earlier than 48 h after irradiation, there is a high probability of obtaining overestimated survival values, because radiation induces an increase in the metabolic

activity of the cell [77]. Over 96 h, the control (non-irradiated) cells complete 3–5 division cycles. This creates the necessary gap in optical density between the control and the treated groups (Irradiation, 5-PVP, BNCT).

According to the migration test data, the cells did not lose their migratory ability, but their morphology in the "BNCT" groups changed after 3 days (Figure 4).

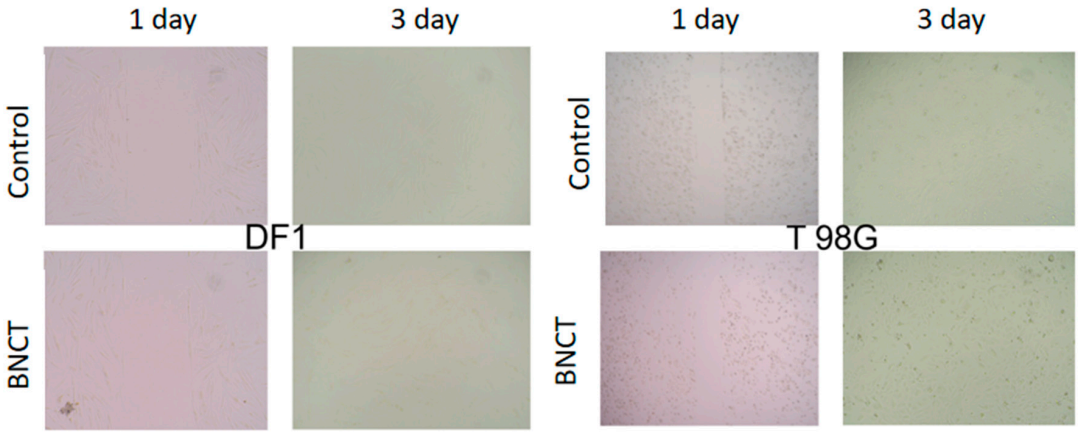


Figure 4. Cell migration assay. Magnification: ×100.

Previous studies have demonstrated that radiation affects tumor cell migration. Since migration is an important stage of tumor metastasis, one of the factors contributing to successful radiation therapy is the inhibition of cell migration under the action of ionizing radiation [78,79].

Figure 5 presents the results of the clonogenic assay. It was found that preincubation with the new boron-containing compound **5-PVP** followed by neutron irradiation reduced the survival of T98G glioblastoma cells to 25% and B16 melanoma cells to 17%. The effect of BNCT on DF1 fibroblasts was less pronounced, with a cloning efficiency of 39%. Although DF1 cells are dermal fibroblasts derived from a healthy donor, this line is immortalized and capable of unlimited division. Nevertheless, the cells retain normal cell cycle control mechanisms and, consequently, are sensitive to radiation exposure.

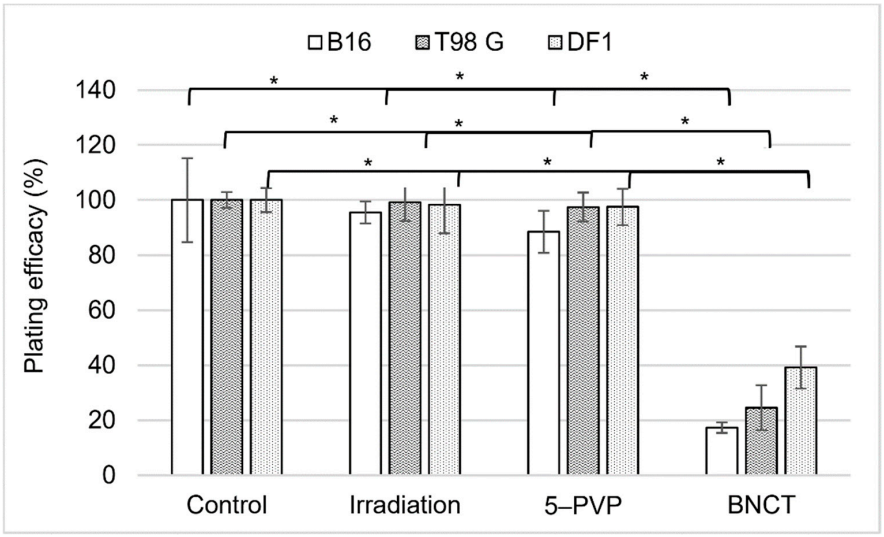


Figure 5. Assessment of the plating efficacy following various treatments by clonogenic assay. *—$p < 0.05$ for differences between the BNCT group and the control/experimental groups (one-way ANOVA followed by Tukey's post-hoc test, $n = 3$ independent experiments).

The difference in the magnitude of the results obtained from the cell-based assays can be explained by the fact that the MTT assay evaluates the metabolic activity of cells, some of which, after exposure to radiation or BNCT, are still considered viable but are unable to proliferate, whereas the clonogenic assay is the gold standard in radiobiology and assesses the number of colonies that have formed in the control and experimental groups [80].

3.2.3. Dosimetry Calculations

To calculate the absorbed dose in a cell suspension volume, we used the computational model of the neutron-generating system (Figure 6a) of the VITA accelerator-based neutron source developed and verified in [68,69] within the Geant4 simulation toolkit (v. 11.2.1) using the QGSP_BIC_AllHP physics list. We supplemented the model with a PMMA phantom holder loaded with cryotubes (Figure 6b) placed on a wooden base. The model geometry closely reproduces the experimental setup used for in vitro experiments (see in Supplementary Materials, Figure S32).

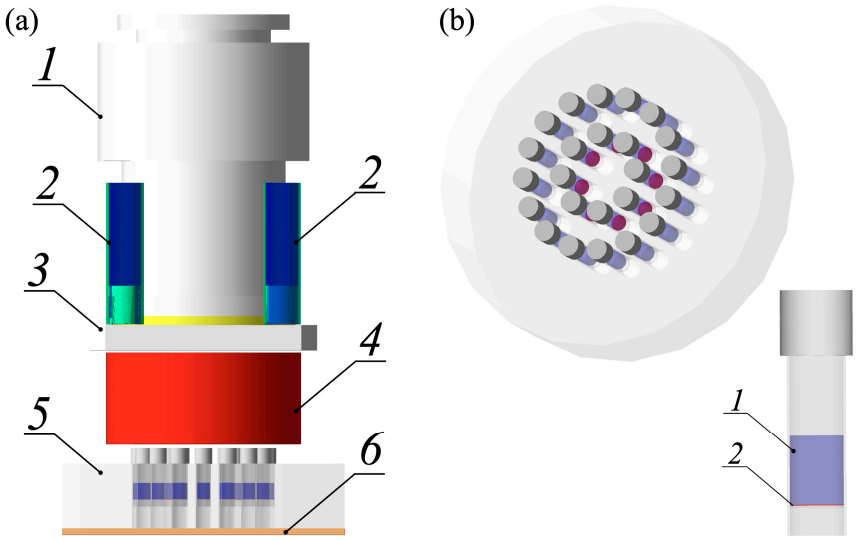


Figure 6. Geometry of the model of the neutron-generating system of the VITA accelerator-based neutron source in Geant4 software toolkit: (**a**) General view of the model: 1—high-energy proton beam transport line, 2—pipes of the target unit cooling system, 3—target unit, 4—Poly-Biz neutron moderator, 5—PMMA phantom holder; (**b**) Model of the PMMA phantom holder loaded with cryotubes at the inner (25 mm) and outer (50 mm) radii: 1—water; 2—cell microlayer.

In accordance with the experimental conditions, in the computational model the cryotubes containing the cell suspension were positioned at the inner radius of the holder, and the cryotubes at the outer radius contained 1 mL of deionized water. The parameters of the irradiated samples in the computational model were set to match the experimental values: a total cell suspension volume of 1 mL and 10^6 cells. For simplicity, water was used as the culture medium, which contains several dozen components, most of them at negligibly low concentrations. The cells were modeled using the ICRU soft tissue composition.

The absorbed dose was calculated using the results of a study on the uptake of **5-PVP**, according to which incubation of the cells followed by washing results in the accumulation of ^{10}B at a concentration of 0.20 μg/10^6 cells. An important factor that must be considered when calculating the absorbed dose is the sedimentation of cells at the bottom of the cryotube within the suspension volume. The absorbed dose is expressed as the ratio of the radiation energy absorbed in each volume to the mass of matter in that volume. It is therefore necessary to determine which volume should be selected as the sensitive volume.

To account for cell sedimentation at the bottom of the cryotube, the sensitive volume was taken not as the entire suspension volume (1 mL) but only as a thin microlayer of the cell suspension that had settled. In this approximation, the volume occupied by 10^6 cells was represented as 10^6 cubes, each containing a spherical cell 20 μm in diameter, assuming a loose, diffuse arrangement of the cells upon sedimentation (see in Supplementary Materials, Figure S33). This approximation is admittedly associated with uncertainty and requires further investigation, e.g., microscopic imaging and other experimental data that would allow the height of the sensitive volume to be determined more accurately. The microlayer at the bottom of the cryotube, considered as the sensitive volume, is shown in red in Figure 6b. The thickness of this microlayer and the ^{10}B concentration in it, calculated as described above, were 102 μm and 24.5 μg/mL, respectively. The remaining part of the suspension, shown as the blue cylinder in Figure 6b, was set as water.

Using the energy-angular spectrum of neutrons generated in the lithium target, 10^9 neutrons were sampled. Finally, the energy deposition in the sensitive volume was normalized using the neutron fluence accumulated at the samples over an exposure time of 30 min at a proton beam current of 2 mA (integrated current, 1 mA × h) and a beam energy of 2.0 MeV. The total absorbed dose, averaged over the eight irradiated cryotubes, was 0.77 ± 0.03 Gy, and its boron component was 0.43 ± 0.03 Gy. The neutron fluence through the cell layer, averaged over the eight irradiated cryotubes, was (1.451 ± 0.001) × 10^{11} cm^{-2}; the energy spectrum is shown in Figure 7.

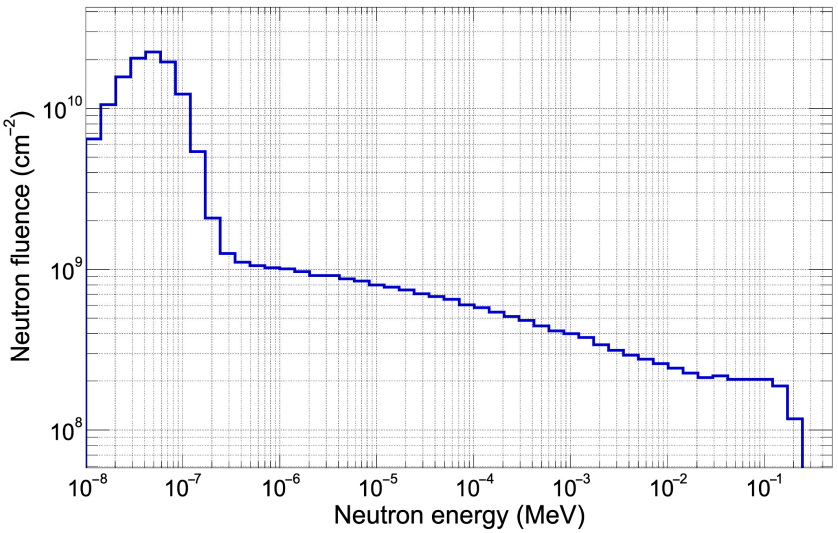


Figure 7. Neutron fluence as a function of neutron energy at the sample position.

3.2.4. Ex Vivo Biodistribution and Tumor Uptake Study of **5-PVP**

An ex vivo biodistribution and tumor uptake study of **5-PVP** was performed in B16F10 melanoma-bearing mice using ICP-OES. Boron concentrations in organs and tissues were measured after a single intravenous injection at a dose of 2.01 ± 0.08 mg B/kg. The resulting time-dependent concentration profiles are presented in Figures 8 and 9.

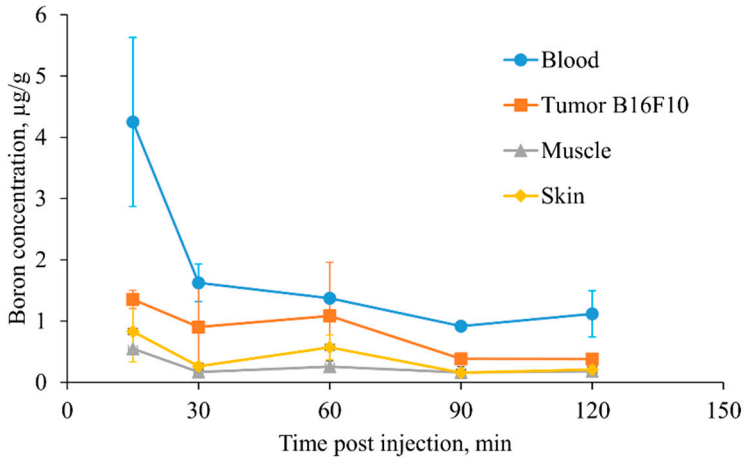


Figure 8. Boron concentration profiles in blood, tumor (B16F10 melanoma), muscle, and skin after a single intravenous injection of **5-PVP**. Data are presented as mean ± SD, $n = 5$ per time point.

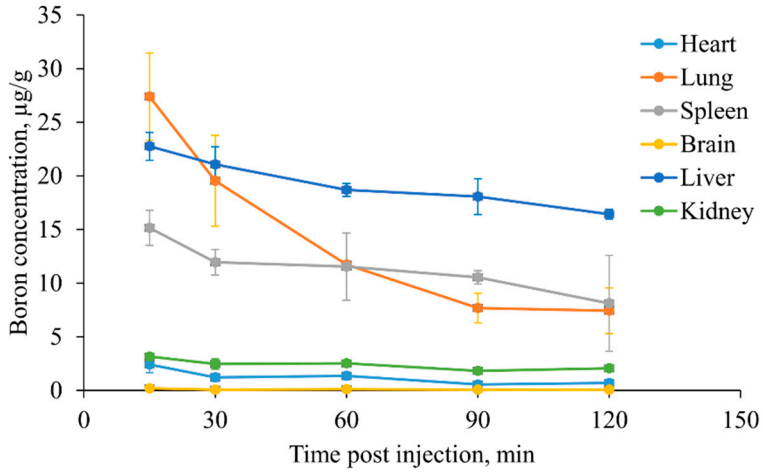


Figure 9. Boron concentration profiles in the heart, lungs, spleen, brain, liver, and kidneys after a single intravenous injection of **5-PVP**. Data are presented as mean ± SD, $n = 5$ per time point.

As expected for intravenous administration, the highest boron concentration in blood was observed at the earliest time point (15 min), with a value of 4.3 ± 1.4 μg B/g. Thereafter, the blood boron level declined rapidly by 30 min, followed by a slight decrease up to 90 min. Between 90 and 120 min, the concentration remained relatively stable, fluctuating around 1.02 ± 0.14 μg B/g.

The highest boron concentration in the tumor was also detected at 15 min post-injection, corresponding to 1.4 ± 0.2 μg B/g, and gradually decreased to 0.4 ± 0.1 μg B/g by 120 min. A slight increase at 60 min was not statistically significant ($p = 0.216$, ANOVA). Overall, the boron concentration profile in the tumor was similar in shape to that in the blood.

The concentration profiles in skin and muscle were also comparable to those in blood and tumor, but with lower absolute values. These findings suggest a relative specificity of **5-PVP** accumulation in the tumor compared to the surrounding normal tissues.

All other healthy organs shown in Figure 9 also exhibited the highest boron concentration at 15 min after administration. The most intense boron accumulation was observed in the lungs, liver, and spleen. In these organs, absolute boron concentrations ranged from 15–27 μg B/g at 15 min to 7–16 μg B/g by 120 min post injection. In the brain, boron levels remained very low throughout the observation period, ranging from 0.20 to 0.06 μg B/g over 120 min. These results suggest that **5-PVP** does not cross the blood–brain barrier, and

that the boron detected in the brain is most likely attributable to the presence of boron in the cerebral blood vessels.

To evaluate the potential of **5-PVP** for boron neutron capture therapy (BNCT), the tumor-to-normal tissue ratios were plotted as a function of time and are presented in Figure 10.

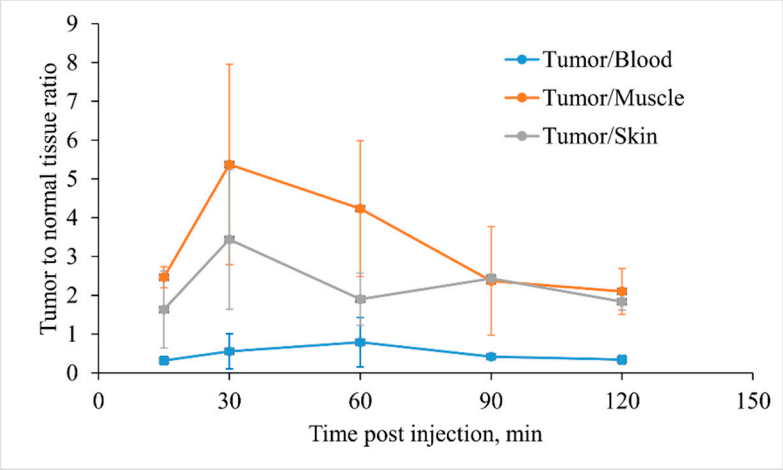


Figure 10. Time course of tumor-to-normal tissue concentration ratios (tumor/blood, tumor/skin, and tumor/muscle) in B16F10 melanoma-bearing mice after a single intravenous injection of **5-PVP**. Data are presented as mean ± SD, $n = 5$ per time point.

The tumor/muscle and tumor/skin ratios reached values of 5.4 and 3.4, respectively, at 30 min post-injection, and gradually decreased to 2.1 and 1.8 by 120 min. Notably, these ratios remained at acceptable levels over a time frame compatible with a BNCT session.

In our previous study [81], we evaluated the accumulation and retention of boronophenylalanine (BPA), the conventional BNCT agent, in tumor-bearing mice. In that work, BPA was administered at a higher boron dose of 28 mg B/kg bw. All other experimental conditions were comparable, including the same B16F10 melanoma model and intravenous administration. Although the BPA data are historical and were obtained at a different dose, relative measures (tumor-to-normal tissue concentration ratios) can be considered for an exploratory comparison of the two compounds. For BPA, the tumor/muscle ratio achieved a maximum of 3 at 30 min post-injection, gradually declined to 1.5 at 90 min, and then remained stable up to 120 min. For **5-PVP**, the tumor/muscle ratio was higher, reaching 5.4 at 30 min. These findings may provide a rationale for further preclinical evaluation of **5-PVP** alongside established BNCT agents.

It should be noted that the absolute boron concentrations achieved in the tumor in the present study (1.4 ± 0.2 μg B/g at 15 min, declining to 0.4 ± 0.1 μg B/g at 120 min) are below the level conventionally regarded as necessary for BNCT, and increasing the boron concentration in the tumor would require a corresponding increase in the administered dose. Since the present work was designed as a fundamental biodistribution study rather than a therapeutic experiment, no dose escalation was performed, and the administered dose (2.01 ± 0.08 mg B/kg) was selected for analytical rather than therapeutic purposes. A dose adjustment will therefore be necessary when progressing to in vivo BNCT studies.

The similar shapes of the concentration–time profiles in blood and tumor indicate that tumor uptake of **5-PVP** is driven primarily by passive mechanisms rather than by active targeting, and the maximum tumor/blood ratio of 0.8 points to a moderate level of bioavailability. However, the absence of active targeting does not preclude the achievement of therapeutic boron concentrations. For example, sodium borocaptate (BSH), which has

been used in clinical BNCT studies for brain tumors, likewise lacks a specific tumor-targeting mechanism, yet it has demonstrated therapeutic potential in this setting.

An alternative approach to achieving therapeutic boron concentrations with non-specific delivery agents is infusion-based administration, which helps to maintain sustained boron levels in the tumor while limiting peak concentrations in normal tissues. In the present proof-of-concept study, **5-PVP** was administered as a single intravenous injection, since infusion in mice is technically challenging due to the small circulating blood volume. Infusion-based administration nevertheless represents a feasible direction for further preclinical evaluation in larger animals such as rats or dogs.

Finally, the elevated boron accumulation observed in the lungs, liver and spleen (15–27 μg B/g at 15 min) should be taken into account when considering the range of potential clinical indications for **5-PVP**. For tumor localizations in which these organs would fall within the neutron irradiation field, such accumulation may restrict the applicability of the compound. This does not apply, however, to the two indications in which BNCT is currently most actively investigated—brain tumors and melanoma of the extremities—since the boron concentrations in muscle, skin and brain were very low, resulting in relatively high tumor-to-normal tissue (T/N) ratios for these tissues. The B16F10 melanoma model used in the present study is clearly more relevant to cutaneous melanoma than to brain tumors. The subcutaneous tumor node is adjacent to skin and muscle tissue, and therefore the tumor/skin and tumor/muscle ratios were selected for analysis. Since the boron concentration in the brain was lower than that in muscle, the tumor/brain ratio would be even higher.

4. Conclusions

A series of novel iodinated cobalt bis(dicarbollide)-acridine conjugates was successfully synthesized *via* direct electrophilic iodination of the parent cobalt bis(dicarbollide)-acridine adducts using molecular iodine as the halogenating agent. The cytotoxic profiles of the newly synthesized compounds were assessed against a panel of human cell lines of diverse origin. Notably, only one of them exhibited no antiproliferative activity against either cancerous or non-malignant cells.

To enhance its aqueous solubility, this iodinated cobalt bis(dicarbollide) conjugate with acridine was subsequently formulated as a non-covalent inclusion complex with polyvinylpyrrolidone. The resulting complex was shown to penetrate cells and accumulate at the boron concentration required for effective BNCT. It was found that preincubation with the new boron-containing compound followed by neutron irradiation reduced the survival of T98G glioblastoma cells to 25% and B16 melanoma cells to 17%.

In vivo study demonstrated a tumor/muscle boron concentration ratio of 5.4 at 30 min post-injection, with the ratio remaining above 2 for up to 120 min in the subcutaneous B16F10 melanoma model. These values support further investigation of the conjugate as a potential boron delivery agent. However, the absolute boron concentrations observed in the tumor were below levels conventionally regarded as sufficient for BNCT. Comparatively high boron accumulation was also recorded in several normal organs, including the lungs, liver and spleen. Future studies may focus on dose escalation to achieve therapeutic boron concentrations in the tumor, optimization of the pharmacokinetic properties and direct comparative evaluation with current clinical BNCT agents.

Supplementary Materials: The following supporting information can be downloaded at: https://www.mdpi.com/article/10.3390/reactions7040064/s1, Figures S1–S8: NMR, IR, and mass spectra of compound **5**; Figures S9–S16: NMR, IR, and mass spectra of compound **6**; Figures S17–S24: NMR, IR, and mass spectra of compound **7**; Figures S25–S31: NMR, IR, and mass spectra of compound **8**; Figures S32–S33: Dosimetry calculations.

Author Contributions: N.V.D.: Formal analysis, Investigation. E.V.S.: Data curation, Investigation. A.I.K.: Formal analysis, Investigation, Writing—original draft. T.A.B.: Formal analysis, Investigation. Y.V.R.: Investigation. D.S.P.: Investigation. A.A.A.: Formal analysis, Investigation. A.A.N.: Formal analysis, Investigation. V.A.S.: Data curation, Investigation, Writing—original draft. A.A.K.: Data curation, Investigation. Y.A.F.: Formal analysis, Writing—original draft. V.I.L.: Conceptualization, Supervision, Writing—review and editing. S.Y.T.: Conceptualization, Supervision. A.A.L.: Conceptualization, Supervision. S.A.A.: Formal analysis, Investigation. A.A.D.: Conceptualization, Formal analysis, Writing—original draft. I.B.S.: Writing—review and editing, Supervision. V.I.B.: Conceptualization, Supervision. All authors have read and agreed to the published version of the manuscript.

Funding: The synthesis and characterization of the new compounds described in this study were supported by the Ministry of Science and Higher Education of the Russian Federation as part of the State Assignment of the A.N. Nesmeyanov Institute of Organoelement Compounds of the Russian Academy of Sciences (075-03-2026-024). The NMR spectra were obtained using equipment of the Center for Molecular Structure Research at the A.N. Nesmeyanov Institute of Organoelement Compounds, supported by the Ministry of Science and Higher Education of the Russian Federation.

Institutional Review Board Statement: All experiments involving laboratory animals were carried out in accordance with the ethical standards for the treatment of animals adopted by the European Convention for the Protection of Vertebrate Animals used for Research and other Scientific Purposes and were approved by the Local Biomedical Ethics Committee (No. 2026-5.1, issued on 15 May 2026).

Data Availability Statement: Data are contained within the article.

Acknowledgments: The authors acknowledge support from the M.V. Lomonosov Moscow State University Program of Development ("Feyond-A400" microplate reader (Allsheng, Hangzhou, China) and "EzMate" automated pipetting system (Blue-Ray Biotech, Taipei, Taiwan)).

Conflicts of Interest: The authors declare no conflicts of interest.

References

1. Sung, H.; Filho, A.M.; Laversanne, M.; Ferlay, J.; Siegel, R.L.; Soerjomataram, I.; Jemal, A.; Bray, B. Global cancer statistics 2024: GLOBOCAN estimates of incidence and mortality worldwide for 34 cancers in 186 countries. *CA Cancer J. Clin.* **2026**, *76*, e70090. [CrossRef]
2. Force, L.; Kocarnik, J.; May, M.; Bhangdia, K.; Crist, A.; Penberthy, L.; Pritchett, N.; Acheson, A.; Deitesfeld, L.; Bhoomadevi, A.; et al. The global, regional, and national burden of cancer, 1990–2023, with forecasts to 2050: A systematic analysis for the Global Burden of Disease Study 2023. *Lancet* **2025**, *406*, 1565–1586. [CrossRef]
3. Seyyedsalehi, M.S.; Boffetta, P. Global cancer statistics 2024: Translating epidemiological trends into priorities for healthcare systems. *Nat. Rev. Clin. Oncol.* **2026**, *23*, 919–920. [CrossRef]
4. Siegel, R.L.; Kratzer, T.B.; Wagle, N.S.; Sung, H.; Jemal, A. Cancer statistics, 2026. *CA Cancer J. Clin.* **2026**, *76*, e70043. [CrossRef]
5. Zhou, L.; Chen, Y.; Peng, M.; Yin, X.; Liang, H.; Mo, J.; Zhang, W.; Liu, Z. Clinical application of boron neutron capture therapy for cancer treatment: A systematic review. *Precis. Radiat. Oncol.* **2025**, *9*, 304–313. [CrossRef]
6. Li, X.; Liu, Z.; Liu, K.; Wang, C.; Liu, Z.; Xu, X. Advances in Clinical Trials of Boron Neutron Capture Therapy. *Research* **2026**, *9*, 0988. [CrossRef]
7. Kashihara, T.; Nakamura, S.; Yamazaki, N.; Takahashi, A.; Namikawa, K.; Ogata, D.; Nakano, E.; Okuma, K.; Kaneda, T.; Mori, T.; et al. Boron neutron capture therapy for cutaneous angiosarcoma and malignant melanoma: First in-human phase I clinical trial. *Radiother. Oncol.* **2025**, *202*, 110607. [CrossRef]
8. Kawabata, S.; Goto, H.; Narita, Y.; Furuse, M.; Nonoguchi, N.; Shidoh-Kazuki, R.; Eza, K.; Hirose, K.; Ohno, M.; Kondo, N.; et al. Extended follow-up of recurrent glioblastoma patients treated with boron neutron capture therapy (BNCT): Long-term survival from a Phase II trial (JG002) using Cyclotron Neutron Source and Boronophenylalanine. *Appl. Radiat. Isot.* **2025**, *226*, 112118. [CrossRef]
9. Zhou, R.; You, Z.; Liu, L. Boron neutron capture therapy in the context of tumor heterogeneity: Progress, challenges, and future perspectives. *Front. Oncol.* **2025**, *15*, 1601013. [CrossRef]
10. Kutuk, T.; Atak, E.; Harrell, M.; Raval, R.R.; Fekrmandi, F.; Zhu, S.; Beyer, S.; Singh, P.K.; Giglio, P.; Mohtashami, H.; et al. Boron Neutron Capture Therapy for High-Grade CNS Tumors: Mechanisms, Carriers, and Clinical Progress: A Narrative Review. *Int. J. Mol. Sci.* **2026**, *27*, 2765. [CrossRef]

11. Tang, D.; Shi, M.; Mao, Z.; Chen, W.; Li, X.; Zhao, X.Y.; Liu, Z.; Xu, X. Boron-10 carriers and their applications in boron neutron capture therapy. *Precis. Radiat. Oncol.* **2026**, *10*, 205–241. [CrossRef]
12. Sauerwein, W. Principles and Roots of Neutron Capture Therapy. In *Neutron Capture Therapy: Principles and Applications*; Springer: Berlin/Heidelberg, Germany, 2012. [CrossRef]
13. Sibrian-Vazquez, M.; Vicente, M.G.H. Boron Tumor-Delivery for BNCT: Recent Developments and Perspectives. In *Boron Science: New Technologies and Applications*; Taylor & Francis: Boca Raton, FL, USA, 2014. [CrossRef]
14. Zhu, Y.; Hosmane, N.S. Applications and perspectives of boron-enriched nanocomposites in cancer therapy. *Future Med. Chem.* **2013**, *5*, 705–714. [CrossRef]
15. Uspenskii, S.A.; Khaptakhanova, P.A. Boron nanoparticles in chemotherapy and radiotherapy: The synthesis, state-of-the-art, and prospects. *Russ. Chem. Bull.* **2022**, *71*, 2533–2560. [CrossRef]
16. Barth, R.F.; Zhang, Z.; Liu, T. A realistic appraisal of boron neutron capture therapy as a cancer treatment modality. *Cancer Commun.* **2018**, *38*, 36. [CrossRef]
17. Xuan, S.; Vicente, M.G.H. Recent Advances in Boron Delivery Agents for Boron Neutron Capture Therapy (BNCT). In *Boron-Based Compounds: Potential and Emerging Applications in Biomedicine*; John Wiley & Sons: Hoboken, NJ, USA, 2018.
18. Oloo, S.O.; Smith, K.M.; Vicente, M.G.H. Multi-functional boron-delivery agents for boron neutron capture therapy of cancers. *Cancers* **2023**, *15*, 3277. [CrossRef]
19. Selg, C.; Hey-Hawkins, E. Boron neutron capture therapy at a crossroads: Translational gap and emerging delivery agents. *Chem. Eur. J.* **2026**, *32*, e03533. [CrossRef]
20. Hawthorne, M.F. The role of chemistry in the development of boron neutron capture therapy of cancer. *Angew. Chem. Int. Ed.* **1993**, *32*, 950–984. [CrossRef]
21. Soloway, A.H.; Tjarks, W.; Barnum, B.A.; Rong, F.G.; Barth, R.F.; Codogni, I.M.; Wilson, J.G. The Chemistry of Neutron Capture Therapy. *Chem. Rev.* **1998**, *98*, 1515–1562. [CrossRef]
22. Scholz, M.; Hey-Hawkins, E. Carbaboranes as Pharmacophores: Properties, Synthesis, and Application Strategies. *Chem. Rev.* **2011**, *111*, 7035–7062. [CrossRef]
23. Hartman, T.; Carlsson, J. Radiation dose heterogeneity in receptor and antigen mediated boron neutron capture therapy. *Radiother. Oncol.* **1994**, *31*, 61–75. [CrossRef]
24. Gabel, D.; Foster, S.; Fairchild, R.G. The Monte Carlo simulation of the biological effect of the $^{10}B(n, \alpha)^{7}Li$ reaction in cells and tissue and its implication for boron neutron capture therapy. *Radiat. Res.* **1987**, *111*, 14–25. [CrossRef]
25. Tjarks, W.; Ghaneolhosseini, H.; Henssen, C.L.; Malmquist, J.; Sjöberg, S. Synthesis of *para*-and *nido*-carboranyl phenanthridinium compounds for neutron capture therapy. *Tetrahedron Lett.* **1996**, *37*, 6905–6908. [CrossRef]
26. Ghaneolhosseini, H.; Tjarks, W.; Sjöberg, S. Synthesis of boronated phenanthridinium derivatives for potential use in boron neutron capture therapy (BNCT). *Tetrahedron* **1997**, *53*, 17519–17526. [CrossRef]
27. Ghaneolhosseini, H.; Sjöberg, S. Synthesis of a boronated naphthalimide for potential use in boron neutron capture therapy (BNCT). *Acta Chem. Scand.* **1999**, *53*, 298–300. [CrossRef]
28. Nekvinda, J.; Różycka, D.; Rykowski, S.; Wyszko, E.; Fedoruk-Wyszomirska, A.; Gurda, D.; Orlicka-Płocka, M.; Giel-Pietraszuk, M.; Kiliszek, A.; Rypniewski, W.; et al. Synthesis of naphthalimide-carborane and metallacarborane conjugates: Anticancer activity, DNA binding ability. *Bioorg. Chem.* **2020**, *94*, 103432. [CrossRef]
29. Rykowski, S.; Gurda-Woźna, D.; Orlicka-Płocka, M.; Fedoruk-Wyszomirska, A.; Giel-Pietraszuk, M.; Wyszko, E.; Kowalczyk, A.; Stączek, P.; Bak, A.; Kiliszek, A.; et al. Design, synthesis, and evaluation of novel 3-carboranyl-1,8-naphthalimide derivatives as potential anticancer agents. *Int. J. Mol. Sci.* **2021**, *22*, 2772. [CrossRef]
30. Bogucka-Kocka, A.; Kołodziej, P.; Makuch-Kocka, A.; Różycka, D.; Rykowski, S.; Nekvinda, J.; Grüner, B.; Olejniczak, A.B. Nematicidal activity of naphthalimide-boron cluster conjugates. *Chem. Commun.* **2022**, *58*, 2528–2531. [CrossRef]
31. Rykowski, S.; Gurda-Woźna, D.; Orlicka-Płocka, M.; Fedoruk-Wyszomirska, A.; Giel-Pietraszuk, M.; Wyszko, E.; Kowalczyk, A.; Stączek, P.; Biniek-Antosiak, K.; Rypniewski, W.; et al. Design of DNA intercalators based on 4-carboranyl-1,8-naphthalimides: Investigation of their DNA-binding ability and anticancer activity. *Int. J. Mol. Sci.* **2022**, *23*, 4598. [CrossRef]
32. Rykowski, S.; Gurda-Woźna, D.; Fedoruk-Wyszomirska, A.; Orlicka-Płocka, M.; Kowalczyk, A.; Stączek, P.; Denel-Bobrowska, M.; Biniek-Antosiak, K.; Rypniewski, W.; Wyszko, E.; et al. Carboranyl-1,8-naphthalimide intercalators induce lysosomal membrane permeabilization and ferroptosis in cancer cell lines. *J. Enzym. Inhib. Med. Chem.* **2023**, *38*, 2171028. [CrossRef]
33. Crossley, E.L.; Ziolkowski, E.J.; Coderre, J.A.; Rendina, L.M. Boronated DNA-binding compounds as potential agents for boron neutron capture therapy. *Mini-Rev. Med. Chem.* **2007**, *7*, 303–313. [CrossRef]
34. Singh, R.; Singh, J.; Kaur, A. Recent Advances in QSAR, SAR, and Therapeutic Potentials of Acridine Derivatives: A Review. *J. Mol. Struct.* **2026**, *1347*, 143226. [CrossRef]
35. Gallala, M.; Tka, N.; Aroui, S. Recent advances in the development of acridine-based hybrids with antiproliferative activity. *RSC Med. Chem.* **2026**, *17*, 2768–2849. [CrossRef]

36. Ghaneolhosseini, H.; Tjarks, W.; Sjöberg, S. Synthesis of novel boronated acridines and spermidines as possible agents for BNCT. *Tetrahedron* **1998**, *54*, 3877–3884. [CrossRef]
37. Różycka, D.; Kowalczyk, A.; Denel-Bobrowska, M.; Kuźmycz, O.; Gapińska, M.; Stączek, P.; Olejniczak, A.B. Acridine/Acridone-Carborane Conjugates as Strong DNA-Binding Agents with Anticancer Potential. *ChemMedChem* **2023**, *18*, e202200666. [CrossRef]
38. Soloway, A.H.; Hatanaka, H.; Davis, M.A. Penetration of brain and brain tumor. VII. Tumor-binding sulfhydryl boron compounds. *J. Med. Chem.* **1967**, *10*, 714–717. [CrossRef]
39. da Silva, A.F.F.; Seixas, R.S.G.R.; Silva, A.M.S.; Coimbra, J.; Fernandes, A.C.; Santos, J.P.; Matos, A.; Rino, J.; Santos, I.; Marques, F. Synthesis, characterization and biological evaluation of carboranylmethylbenzo[*b*]acridones as novel agents for boron neutron capture therapy. *Org. Biomol. Chem.* **2014**, *12*, 5201–5211. [CrossRef]
40. Belchior, A.; Fernandes, A.; Lamotte, M.; da Silva, A.F.F.; Seixas, R.S.G.R.; Silva, A.M.S.; Marques, F. Exploring the physical and biological aspects of BNCT with a carboranylmethylbenzo[*b*]acridone compound in U87 glioblastoma cells. *Int. J. Mol. Sci.* **2022**, *23*, 14929. [CrossRef]
41. Cebula, J.; Fink, K.; Goldeman, W.; Szermer-Olearnik, B.; Nasulewicz-Goldeman, A.; Psurski, M.; Cuprych, M.; Kędziora, A.; Dudek, B.; Bugla-Płoskońska, G.; et al. Structural Patterns Enhancing the Antibacterial Activity of Metallacarborane-Based Antibiotics. *J. Med. Chem.* **2023**, *66*, 14948–14962. [CrossRef]
42. Housecroft, C.E. Boron: Metallacarbaboranes. In *Encyclopedia of Inorganic and Bioinorganic Chemistry*; John Wiley & Sons: New York, NY, USA, 2011. [CrossRef]
43. Dash, B.P.; Satapathy, R.; Swain, B.R.; Mahanta, C.S.; Jena, B.B.; Hosmane, N.S. Cobalt bis(dicarbollide) anion and its derivatives. *J. Organomet. Chem.* **2017**, *849*, 170–194. [CrossRef]
44. Dudarova, N.V.; Kosenko, I.D.; Maltseva, V.E.; Ananyev, I.V.; Druzina, A.A.; Bregadze, V.I.; Sivaev, I.B. On the Issue of Biological Activity of Cobalt bis(dicarbollide) Derivatives: Conformation of the [8-EtO-8′-I-3,3′-Co(1,2-$C_2B_9H_{10}$)$_2$]$^-$ Anion. *J. Clust. Sci.* **2025**, *36*, 161. [CrossRef]
45. Nuez-Martinez, M.; Pinto, C.I.G.; Guerreiro, J.F.; Mendes, F.; Marques, F.; Muñoz-Juan, A.; Xavier, J.A.M.; Laromaine, A.; Bitonto, V.; Protti, N.; et al. Cobaltabis(dicarbollide) ([*o*-COSAN]$^-$) as multifunctional chemotherapeutics: A prospective application in boron neutron capture therapy (BNCT) for glioblastoma. *Cancers* **2021**, *13*, 6367. [CrossRef]
46. Gos, M.; Cebula, J.; Goszczyński, T.M. Metallacarboranes in medicinal chemistry: Current advances and future perspectives. *J. Med. Chem.* **2024**, *67*, 8481–8501. [CrossRef]
47. Bennour, I.; Ramos, M.N.; Nuez-Martínez, M.; Xavier, J.A.M.; Buades, A.B.; Sillanpää, R.; Teixidor, F.; Choquesillo-Lazarte, D.; Romero, I.; Martinez-Medina, M.; et al. Water soluble organometallic small molecules as promising antibacterial agents: Synthesis, physical-chemical properties and biological evaluation to tackle bacterial infections. *Dalton Trans.* **2022**, *51*, 7188–7209. [CrossRef]
48. Fuentes, I.; García-Mendiola, T.; Sato, S.; Pita, M.; Nakamura, H.; Lorenzo, E.; Teixidor, F.; Marques, F.; Viñas, C. Metallacarboranes on the Road to Anticancer Therapies: Cellular Uptake, DNA Interaction, and Biological Evaluation of Cobaltabisdicarbollide [COSAN]$^-$. *Chem. Eur. J.* **2018**, *24*, 17239–17254. [CrossRef]
49. Tarrés, M.; Canetta, E.; Paul, E.; Forbes, J.; Azzouni, K.; Viñas, C.; Teixidor, F.; Harwood, A.J. Biological interaction of living cells with COSAN-based synthetic vesicles. *Sci. Rep.* **2015**, *5*, 7804. [CrossRef]
50. Spryshkova, R.A.; Karaseva, L.I.; Brattsev, V.A.; Serebriakov, N.G. Toxicity of the functional derivatives of polyhedral carboranes. *Med. Radiol.* **1981**, *26*, 62–64. [PubMed]
51. Bauduin, P.; Prevost, S.; Farràs, P.; Teixidor, F.; Diat, O.; Zemb, T. A theta-shaped amphiphilic cobaltabisdicarbollide anion: Transition from monolayer vesicles to micelles. *Angew. Chem. Int. Ed.* **2011**, *50*, 5298–5300. [CrossRef]
52. Verdiá-Báguena, C.; Alcaraz, A.; Aguilella, V.M.; Cioran, A.M.; Tachikawa, S.; Nakamura, H.; Teixidor, F.; Viñas, C. Amphiphilic COSAN and I_2-COSAN crossing synthetic lipid membranes: Planar bilayers and liposomes. *Chem. Commun.* **2014**, *50*, 6700–6703. [CrossRef]
53. Chaari, M.; Gaztelumendi, N.; Cabrera-Gonzalez, J.; Peixoto-Moledo, P.; Vinas, C.; Xochitiotzi-Flores, E.; Farfán, N.; Ben Salah, A.; Nogués, C.; Nunez, R. Fluorescent BODIPY-Anionic Boron Cluster Conjugates as Potential Agents for Cell Tracking. *Bioconjugate Chem.* **2018**, *29*, 1763–1773. [CrossRef]
54. Ferrer-Ugalde, A.; Muñoz-Juan, A.; Laromaine, A.; Curotto, P.; Nievas, S.; Dagrosa, M.A.; Couto, M.; Núñez, R. Enhancing Boron Neutron Capture Therapy (BNCT) with Materials Based on COSAN-Functionalized Nanoparticles. *Pharmaceuticals* **2025**, *18*, 466. [CrossRef]
55. Llop, J.; Masalles, C.; Viñas, C.; Teixidor, F.; Sillanpää, R.; Kivekäs, R. The [3,3′-Co(1,2-$C_2B_9H_{11}$)$_2$]$^-$ anion as a platform for new materials: Synthesis of its functionalized monosubstituted derivatives incorporating synthons for conducting organic polymers. *Dalton Trans.* **2003**, *32*, 556–561. [CrossRef]
56. Assaf, K.I.; Begaj, B.; Frank, A.; Nilam, M.; Mougharbel, A.S.; Kortz, U.; Nekvinda, J.; Grüner, B.; Gabel, D.; Nau, W.M. High-Affinity Binding of Metallacarborane Cobalt Bis(dicarbollide) Anions to Cyclodextrins and Application to Membrane Translocation. *J. Org. Chem.* **2019**, *84*, 11790–11798. [CrossRef]

57. Zakret-Drozdowska, K.; Szermer-Olearnik, B.; Goldeman, W.; Gos, M.; Drozdowski, D.; Gągor, A.; Goszczyński, T.M. Unraveling the correlation between biological effects and halogen substituents in cobalt bis(dicarbollide). *Inorg. Chem. Front.* **2025**, *12*, 191–204. [CrossRef]
58. Sivaev, I.B.; Kosenko, I.D. Rotational conformation of 8,8′-dihalogenated derivatives of cobalt bis(dicarbollide) in solution. *Russ. Chem. Bull.* **2021**, *70*, 753–756. [CrossRef]
59. Rokitskaya, T.I.; Kosenko, I.D.; Sivaev, I.B.; Antonenko, Y.N.; Bregadze, V.I. Fast flip-flop of halogenated cobalt bis(dicarbollide) anion in a lipid bilayer membrane. *Phys. Chem. Chem. Phys.* **2017**, *19*, 25122–25128. [CrossRef]
60. Swietnicki, W.; Goldeman, W.; Psurski, M.; Nasulewicz-Goldeman, A.; Boguszewska-Czubara, A.; Drab, M.; Sycz, J.; Goszczyński, T.M. Metallacarborane derivatives effective against *Pseudomonas aeruginosa* and *Yersinia enterocolitica*. *Int. J. Mol. Sci.* **2021**, *22*, 6762. [CrossRef]
61. Ferrer-Ugalde, A.; Sandoval, S.; Pulagam, K.R.; Muñoz-Juan, A.; Laromaine, A.; Llop, J.; Tobias, G.; Núñez, R. Radiolabeled cobaltabis (dicarbollide) anion–graphene oxide nanocomposites for in vivo bioimaging and boron delivery. *ACS Appl. Nano Mater.* **2021**, *4*, 1613–1625. [CrossRef]
62. Gona, K.B.; Zaulet, A.; Gómez-Vallejo, V.; Teixidor, F.; Llop, J.; Viñas, C. COSAN as a molecular imaging platform: Synthesis and "in vivo" imaging. *Chem. Commun.* **2014**, *50*, 11415–11417. [CrossRef]
63. Druzina, A.A.; Dudarova, N.V.; Ananyev, I.V.; Antonets, A.A.; Kaluzhny, D.N.; Nazarov, A.A.; Sivaev, I.B.; Bregadze, V.I. New Boron Containing Acridines: Synthesis and Preliminary Biological Study. *Molecules* **2023**, *28*, 6636. [CrossRef]
64. Laskova, J.; Serdyukov, A.; Kosenko, I.; Ananyev, I.; Titova, E.; Druzina, A.; Sivaev, I.; Antonets, A.A.; Nazarov, A.A.; Bregadze, V.I. New azido coumarins as potential agents for fluorescent labeling and their "click" chemistry reactions for the conjugation with *closo*-dodecaborate anion. *Molecules* **2022**, *27*, 8575. [CrossRef]
65. Kumar, P.; Nagarajan, A.; Uchil, P.D. Analysis of Cell Viability by the MTT Assay. *Cold Spring Harb. Protoc.* **2018**. [CrossRef]
66. Ghasemi, M.; Turnbull, T.; Sebastian, S.; Kempson, I. The MTT Assay: Utility, Limitations, Pitfalls, and Interpretation in Bulk and Single-Cell Analysis. *Int. J. Mol. Sci.* **2021**, *22*, 12827. [CrossRef]
67. Taskaev, S.; Berendeev, E.; Bikchurina, M.; Bykov, T.; Chesnokova, Y.; Deeb, R.; Ibrahim, I.; Kasatova, A.; Kasatov, D.; Kolesnikov, Y.; et al. VITA accelerator neutron sources: Status and research results. *Cancers* **2026**, *18*, 1886. [CrossRef]
68. Azarkin, M.Y.; Zavestovskaya, I.N.; Kirakosyan, M.R.; Petrunya, D.S.; Kasatov, D.A.; Konovalova, V.D.; Taskaev, S.Y. Evaluation of Neutron Field Parameters at the VITA Facility Using Geant4 Simulation. *Bull. Lebedev Phys. Inst.* **2025**, *52*, 72–78. [CrossRef]
69. Petrunya, D.S.; Azarkin, M.Y.; Zavestovskaya, I.N.; Kasatov, D.A.; Kirakosyan, M.R.; Razdrogova, Y.V.; Taskaev, S.Y. Assessment of absorbed dose distribution for the in vitro setup at the VITA. *Tech. Phys. Lett.* **2026**, *52*, 61–63. [CrossRef]
70. Chilin, A.; Marzaro, G.; Marzano, C.; Dalla Via, L.; Ferlin, M.G.; Pastorini, G.; Guiotto, A. Synthesis and antitumor activity of novel amsacrine analogs: The critical role of the acridine moiety in determining their biological activity. *Bioorg. Med. Chem.* **2009**, *17*, 523–529. [CrossRef]
71. Lang, X.; Li, L.; Chen, Y.; Sun, Q.; Wu, Q.; Liu, F.; Tan, C.; Liu, H.; Gao, C.; Jiang, Y. Novel synthetic acridine derivatives as potent DNA-binding and apoptosis-inducing antitumor agents. *Bioorg. Med. Chem.* **2013**, *21*, 4170–4177. [CrossRef]
72. Tonelli, M.; Vettoretti, G.; Tasso, B.; Novelli, F.; Boido, V.; Sparatore, F.; Busonera, B.; Ouhtit, A.; Farci, P.; Blois, S.; et al. Acridine derivatives as anti-BVDV agents. *Antivir. Res.* **2011**, *91*, 133–141. [CrossRef]
73. Rak, J.; Kaplánek, R.; Král, V. Solubilization and deaggregation of cobalt bis(dicarbollide) derivatives in water by biocompatible excipients. *Bioorg. Med. Chem. Lett.* **2010**, *20*, 1045–1048. [CrossRef]
74. Rak, J.; Jakubek, M.; Kaplánek, R.; Matejícek, P.; Král, V. Cobalt bis(dicarbollide) derivatives: Solubilization and self-assembly suppression. *Eur. J. Med. Chem.* **2011**, *46*, 1140–1146. [CrossRef]
75. Lozinsky, V.I.; Ivanov, R.V.; Kravchenko, D.V.; Ivaschenko, A.A. Composition for Making Dosage Form with Prolonged Effect and Method of Making Said Form. Russian Federation Patent No. 2363451, 14 September 2007.
76. Ivanov, R.V.; Lozinsky, V.I.; Balakin, K.V.; Bachurin, S.O. Pharmaceutical Composition Based on Hydrogenated Pyrido(4,3-b)indole for Treatment of Neurodegenerative Diseases, Method for Preparation of the Composition and Pharmacological Dosage Form on the Basis of This Composition. Russian Federation Patent No. 2428185, 29 December 2009.
77. Rai, Y.; Pathak, R.; Kumari, N.; Sah, D.K.; Pandey, S.; Kalra, N.; Soni, R.; Dwarakanath, B.S.; Bhatt, A.N. Mitochondrial biogenesis and metabolic hyperactivation limits the application of MTT assay in the estimation of radiation induced growth inhibition. *Sci. Rep.* **2018**, *8*, 1531. [CrossRef]
78. Kitabatake, K.; Kaji, T.; Tsukimoto, M. Involvement of CD73 and A2B receptor in radiation-induced DNA damage response and cell migration in human glioblastoma A172 cells. *Biol. Pharm. Bull.* **2021**, *44*, 197–210. [CrossRef]
79. Imaizumi, N.; Monnier, Y.; Hegi, M.; Mirimanoff, R.O.; Rüegg, C. Radiotherapy suppresses angiogenesis in mice through TGF-βRI/ALK5-dependent inhibition of endothelial cell sprouting. *PLoS ONE* **2010**, *5*, e11084. [CrossRef]

80. Banasiak, D.; Barnetson, A.R.; Odell, R.A.; Mameghan, H.; Russell, P.J. Comparison between the clonogenic, MTT, and SRB assays for determining radiosensitivity in a panel of human bladder cancer cell lines and a ureteral cell line. *Radiat. Oncol. Investig.* **1999**, *7*, 77–85. [CrossRef]
81. Ryabchikova, M.N.; Nelyubin, A.V.; Klyukin, I.N.; Selivanov, N.A.; Bykov, A.Y.; Kubasov, A.S.; Skribitsky, V.A.; Finogenova, Y.A.; Shpakova, K.E.; Kasianov, A.A.; et al. Synthesis of New Promising BNCT Agents Based on Conjugates of *closo*-Dodecaborate Anion and Aliphatic Diamino Acids. *Int. J. Mol. Sci.* **2025**, *26*, 68. [CrossRef]

Disclaimer/Publisher's Note: The statements, opinions and data contained in all publications are solely those of the individual author(s) and contributor(s) and not of MDPI and/or the editor(s). MDPI and/or the editor(s) disclaim responsibility for any injury to people or property resulting from any ideas, methods, instructions or products referred to in the content.